on the circum-Pacific terrane map. These relations may indicate physical properties that render seamounts and pelagic sediment to be more susceptible to subduction, continental underplating, recycling into the mantle, or both.

The percentages of terrigenous sediment and volcanic debris in the Pacific Ocean and in the circum-Pacific terranes are rough equivalents lending credence to the hypothesis that continents are growing. On a global scale, terrigenous debris accounts for a bigger percentage, up to 42%. This reflects the large accumulation of sediment along trailing margins (Indian and Atlantic oceans). Even though this material is destined for accretion following a Wilson cycle-like ocean closure, the margin of Panthalassa must not have included major portions of long-lived passive plate regimes.

The total area of the circum-Pacific consisting of terranes accreted since 200 million years ago is approximately $33 \times 10^6$ km$^2$ (*15*). Assuming an average crustal thickness of 20 km, one calculates an accretionary rate of 3.3 km$^3$ per year since the breakup of Pangaea. This value is too large for a continental growth estimate because recycled sediment as well as terranes older than 200 million years are included in the volume calculation. Not until we know the thickness of all terranes younger than 200 million years and can determine the amount of material that is subducted into the mantle will we be able to precisely calculate the rate of continental growth; at this point, the estimates of 3.0 km$^3$ per year for accretion and 1.35 km$^3$ per year for continental growth provide a framework for discussion.


REFERENCES AND NOTES

1. A. Reymer and G. Schubert, *Tectonics* **3**, 63 (1984).
2. C. J. Allegre, *Tectonophysics* **81**, 109 (1982).
3. S. M. McLennan and S. R. Taylor, *J. Geol.* **90**, 347 (1982).
4. R. K. O'Nions *et al.*, *J. Geophys. Res.* **84**, 6091 (1979).
5. J. Veizer and S. L. Jansen, *J. Geol.* **87**, 341 (1979).
6. J. G. Sclater *et al.*, *J. Geophys. Res.* **86**, 11535 (1981).
7. D. E. Karig and R. W. Kay, *Philos. Trans. R. Soc. London Ser. A* **301**, 233 (1981).
8. R. W. Kay, *J. Geol.* **88**, 497 (1980).
9. K. J. Miskell *et al.*, *Bull. Am. Assoc. Pet. Geol.* **69**, 996 (1985).
10. E. L. Hamilton, *J. Sediment. Petrol.* **46**, 280 (1976).
11. J. Sloan, unpublished data.
12. B. Baldwin and C. O. Butler, *Bull. Am. Assoc. Pet. Geol.* **69**, 622 (1985).
13. M. Leinen, *Geochim. Cosmochim. Acta* **41**, 671 (1977).
14. J. D. Milliman and R. H. Meade, *J. Geol.* **91**, 1 (1983).
15. D. G. Howell *et al.*, American Association of Petroleum Geologists, Tulsa, OK, (1985), scale 1:17000000.
16. E. R. Schermer, D. G. Howell, D. L. Jones, *Annu. Rev. Earth Planet. Sci.* **12**, 107 (1984).
17. J. C. Moore, *Geology* **3**, 350 (1975).
18. K. O. Emery and E. Uchupi, *The Geology of the Atlantic Ocean* (Springer-Verlag, New York, 1984).
19. W. J. Ludwig and R. E Houtz, American Association for Petroleum Geologists, Tulsa, OK, (1979), scale 1:15000000.
20. B. E. Tucholke *et al.*, *Bull. Am. Assoc. Pet. Geol.* **66**, 1384 (1982).
21. G. B. Udintsev *et al.*, Eds., *Geological-Geophysical Atlas of the Indian Ocean* (Pergamon, New York, 1975).


22. We thank G. McHendrie and S. Fox for their computer assistance and T. Wiley for helpful discussion. We are grateful to J. Sloan for allowing use of his unpublished carbonate accumulation rates (supported by NSF grant OCE8409369). Suggestions by R. Stanley and D. Rubin improved the clarity of early drafts. This work was partially funded by USGS/DOE interagency agreement DE-AI21-83-MC20422.

27 January 1986; accepted 8 May 1986


# The 1985 Central Chile Earthquake: A Repeat of Previous Great Earthquakes in the Region?


D. Comte, A. Eisenberg, E. Lorca, M. Pardo, L. Ponce, R. Saragoni, S. K. Singh, G. Suárez



**A great earthquake (surface-wave magnitude, 7.8) occurred along the coast of central Chile on 3 March 1985, causing heavy damage to coastal towns. Intense foreshock activity near the epicenter of the main shock occurred for 11 days before the earthquake. The aftershocks of the 1985 earthquake define a rupture area of 170 by 110 square kilometers. The earthquake was forecast on the basis of the nearly constant repeat time (83 ± 9 years) of great earthquakes in this region. An analysis of previous earthquakes suggests that the rupture lengths of great shocks in the region vary by a factor of about 3. The nearly constant repeat time and variable rupture lengths cannot be reconciled with time- or slip-predictable models of earthquake recurrence. The great earthquakes in the region seem to involve a variable rupture mode and yet, for unknown reasons, remain periodic. Historical data suggest that the region south of the 1985 rupture zone should now be considered a gap of high seismic potential that may rupture in a great earthquake in the next few tens of years.**


Central Chile, between 32° and 35°S, has been the site of great earthquakes in 1575, 1647, 1730, 1822, and 1906. This sequence gives a remarkably constant return period of 83 ± 9 (mean ± SD) years for great shocks in the region. On the basis of this sequence and the validity of time- and slip-predictable models of earthquake recurrence, the region had been identified as a gap of high seismic potential, and a great earthquake had been forecast for this decade (*1–3*).

On 3 March 1985 (22:46:56.8 GMT) the central Chilean coast was struck by a great earthquake (surface-wave magnitude, $M_s$ = 7.8), which caused serious damage to the coastal towns from Quintero in the north to Matanza in the south (distance of about 150 km) as well as to many inland towns and cities including Santiago (Fig. 1) (*4*). The earthquake appears to have fulfilled the forecast if we ignore an earthquake in 1971 ($M_s$ = 7.9) that broke the northern one-third of the estimated rupture length of the 1906 shock.

To explain the periodic sequence of the great shocks, the currently popular time- and slip-predictable models of earthquake recurrence (*5*, *6*) require nearly constant rupture lengths. Our analysis of the data, however, shows that the great earthquakes in the region are not similar to each other; their rupture lengths vary by a factor of about 3. The great shocks of central Chile demonstrate that our understanding of the earthquake generation process is still very rudimentary and that there may not be a single universal model valid for all seismic regions of the world.

The main shock of 3 March 1985 was preceded by intense foreshock activity, which began with an event of bodywave magnitude ($m_b$) of 4.7 on 21 February at 18:53:08.5 GMT. The frequency of the foreshocks caused great alarm in Valparaíso (*7*). In the next 11 days the permanent central Chilean network recorded 360 earthquakes with coda magnitudes ($M_c$) of >3.0 (*8*) (Fig. 1). On 2 March 1985 the water wells serving a community near the coast of


D. Comte, A. Eisenberg, M. Pardo, Departamento de Geología y Geofísica, Universidad de Chile, Santiago, Chile.
E. Lorca, Instituto Hidrográfico de la Armada, Valparaíso, Chile.
L. Ponce and G. Suárez, Instituto de Geofísica, Ciudad Universitaria, Universidad Nacional Autónoma de México, 04510 México, DF.
R. Saragoni, Departamento de Ingeniería, Civil, Universidad de Chile, Santiago, Chile.
S. K. Singh, Instituto de Geofísica and Instituto de Ingeniería, Ciudad Universitaria, Universidad Nacional Autónoma de México, 04510 México, DF.

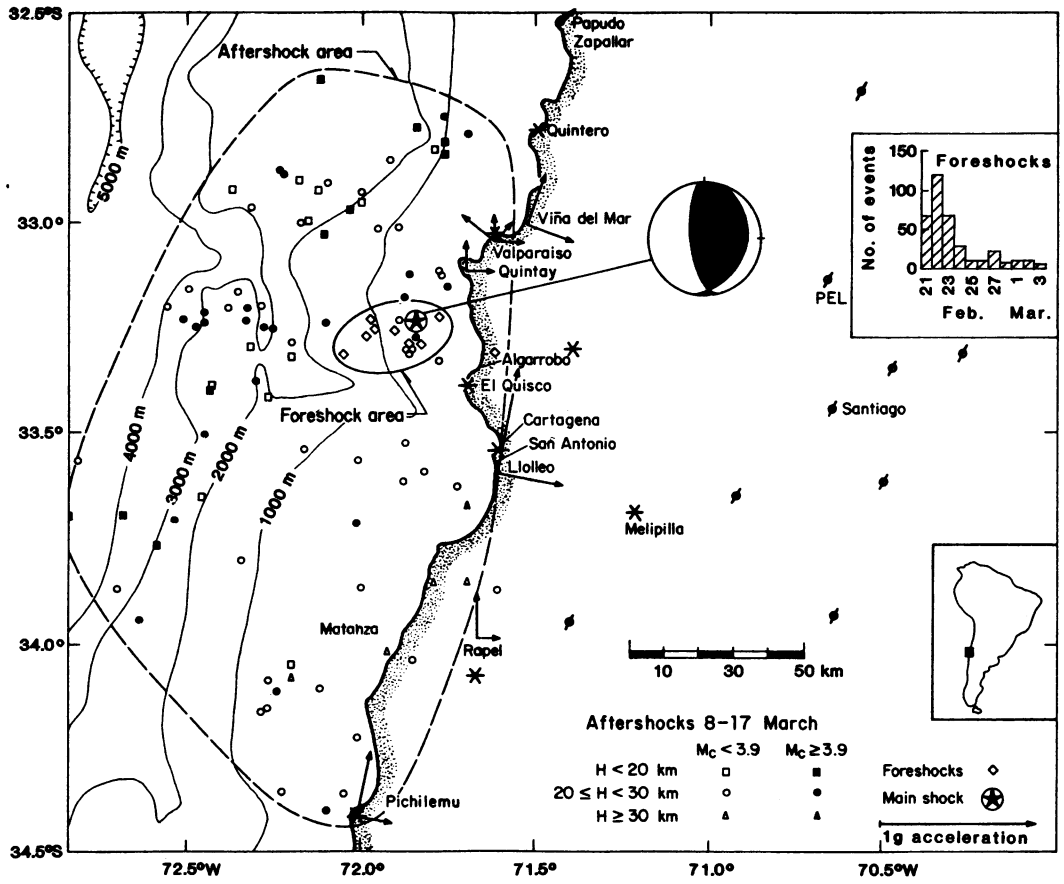


Fig. 1. Map showing the foreshock and aftershock areas and the main shock location of the 3 March 1985 earthquake. The foreshocks and the main shock were located by the permanent central Chile network of seismographs (shown by ϕ); in the aftershock areas the data from portable seismographs (shown by *) were also used. The preferred fault plane, from the focal mechanism (*12*), has strike, dip, and rake of 11°, 25°, and 110°, respectively. The foreshock statistics ($M_c$, ≥3.0) of the earthquake of 21 February ($m_b$, 4.7) are shown at the upper right. Peak horizontal acceleration at coastal sites is shown by vectors whose magnitudes (zero to peak) can be read from the scale at the lower right. The damage along the coast extended from Quintero to Matanza with San Antonio and Llolleo most severely hit. The rupture area estimated from the locations of the events from 8 to 17 March is about 170 by 110 km$^2$. Bathymetry data were provided by the Instituto Hidrográfico de la Armada, Chile. H, depth of aftershock in kilometers.

San Antonio went dry (*9*). The epicenter of the main shock (33.24°S, 71.85°W), determined from the central Chilean network data (*10*), falls in the epicentral area defined by ten precursory events (Fig. 1) chosen for analysis (*11*). Thus, the main shock began in the region of precursory cluster of the foreshock activity about 30 km offshore of Algarrobo (Fig. 1). The focal mechanism of the main shock (Fig. 1) (*12*) is consistent with thrust faulting on a shallow plane dipping 25°. A few long-period *P*-wave records from teleseismic stations show that the main shock consisted of two subevents (Fig. 2). The time difference between the two subevents appears nearly constant at all the stations, and the pulses associated with the second subevent are narrower at stations to the south compared with stations to the north (Fig. 2). From these data we conclude that the two subevents had nearly the same hypocenter and that the larger second subevent propagated to the south. Further support for these conclusions comes from (i) clear accelerograms from Viña del Mar, Llolleo, and Melipilla (Fig. 1) that show two large arrivals of *S* waves about 12.8 seconds apart on all these stations, and (ii) damage and peak horizontal accelerations (Fig. 1) that were larger to the south of the epicenter of the main shock than to the north (*13*).

The earthquake caused tsunami, a great sea wave, along the coast near the focal region, which indicated vertical displacement of the sea floor (*14*). The tide gauges at Valparaíso and San Antonio show a permanent uplift of the shoreline of 11 and 28 cm (±5 cm), respectively. These estimates of uplift are obtained from the predicted value of sea level at these two localities.

Aftershocks were recorded by eight portable smoked-paper field seismographs deployed along the coast and ten permanent stations of the central Chilean network (Fig. 1). The installation of the portable seismographs began on 6 March and was completed by 8 March. All these units were in operation until 16 March. From 17 to 24 March only two portable seismographs, at the northern (Valparaíso) and southern (Pichilemu) ends of the aftershock area, were left in the field. The locations of the portable seismographs complemented the permanent array, which lacks stations along the coast. Figure 1 gives locations of 91 aftershocks occurring between 8 and 17 March, which had coda duration >150 seconds at the seismograph station at Peldehue (PEL). An average of 16 *P*- and 8 *S*-wave readings were available for each event. We located the events by using a flat-layer model appropriate for the coastal region with corrections for inland permanent stations (*11*). The locations in Fig. 1 define an aftershock area of about 170 by 110 km$^2$ (*15*). This aftershock region provides a rough estimate of the rupture area of the main shock, although the actual rupture area may have been somewhat smaller. The location of the main shock with respect to the aftershock area in

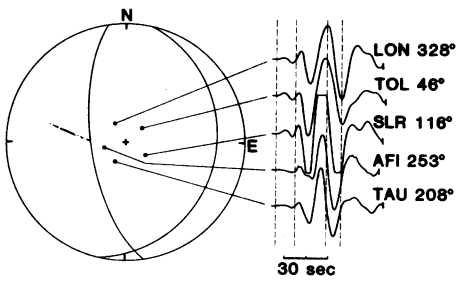


Fig. 2. Long-period *P*-wave records of the 3 March 1985 earthquake from some Digital World-Wide Standard Seismograph Network stations. The station locations, indicated on the right, are shown on an equal-area projection of the lower focal hemisphere. The records suggest that the main shock consisted of two subevents, both of which nucleated at approximately the same hypocenter. The records to the south exhibit narrower pulses for the second subevent compared with those to the north, implying that the second subevent propagated to the south. This source directivity is also supported by the damage distribution, the recorded peak accelerations along the coast, and the extent of the aftershock area with respect to the main shock epicenter (Fig. 1).

Fig. 1 suggests that the rupture propagated 60 km to the north and about 110 km to the south, which gives further evidence of directivity of the source toward the south. The seismic moment, $M_0$, of the earthquake is $1.15 \times 10^{28}$ dyne-cm, which gives a moment-magnitude $M_w$ of 8.0 (*16*). If an area of rupture $A = 170$ by 110 km$^2$ and the rigidity $\mu = 5 \times 10^{11}$ dyne/cm$^2$, then the relation $M_0 = \mu A\bar{u}$ yields the average displacement on the fault $\bar{u}$ of 123 cm.

The Great Valparaíso earthquake of 16 August 1906, which caused severe damage (Mercalli intensities >VIII) (*17*) in a region about 365 km long, extending from Illapel (31.7°S) to Curepto (35°S) (Fig. 3), has been exhaustively studied and reported (*18–21*). These reports seem to suggest that the earthquake started north of Valparaíso (perhaps near La Ligua) and that it was a complex event. The main shock was preceded by precursory activity which began on 18 June with an earthquake that was felt with "extraordinary intensity" in Valparaíso and Santiago (*21*). Although many small shocks were reported, the earthquakes of 20 July, 2 August, and 14 August were felt with Rossi-Forel intensities of IV to V (*21*). Uplift of the coastline of 80 cm (at Zapallar) to 40 cm (at Llico), as a consequence of the main shock, is well documented (*18, 22*). Abe and Noguchi (*23*) have revised the surface-wave magnitude of this earthquake, which, in accordance with the current definition of $M_s$, is 8.3. Our estimate of the magnitude, based on a reexamination of the seismograms, is 8.2 (*24*), which is close to the value given by Abe and Noguchi (*23*). From tsunami data at Hilo, Honolulu, and Japan, Abe (*25*) estimated a tsunami magnitude, $M_t$, of 8.4, which corresponds to a seismic moment of $4 \times 10^{28}$ dyne-cm. After calibration with respect to the 3 March 1985 and 22 May 1960 Chilean earthquakes whose tsunami heights and seismic moments are known (*16, 25–27*), our reestimated value of the seismic moment of the 1906 earthquake is $6.6 \times 10^{28}$ dyne-cm ($M_t = 8.5$) (*28*). If we assume a rupture length of 365 km and a fault width of 150 km, the estimated $\bar{u}$ during the 1906 earthquake was 241 cm.

A space-time plot of large central Chilean earthquakes is shown in Fig. 3. This plot is similar to Kelleher's (*1*). Rupture lengths and locations of earthquakes in previous centuries are based on a reexamination of reports (*18–20, 29, 30*). The larger earthquakes in the region of interest occurred in 1647, 1730, 1822, and 1906 (Fig. 3). The 1575 earthquake is poorly documented, so its size and location are more uncertain than those for other events. The earthquake of 1647 appears similar in size and location to the 1906 Valparaíso earthquake. We estimate the rupture length of the 1730 earthquake as 550 km (*31*). The damage and tsunami reports leave little doubt that this was the largest earthquake in the region (*19, 20*). The southern limit of the rupture zone of the 1822 earthquake is somewhat uncertain (*32*). It may have extended farther south than Melipilla, which was left in ruins. In 1822, the shoreline near Quintero and Valparaíso was uplifted 1.2 m and 0.9 m, respectively (*29, 33*), and precursory earthquakes were felt in Valparaíso beginning 5 days before the main shock (*29*).

The sequence of 1575, 1647, 1730, 1822, and 1906 gives a recurrence period of 83 ± 9 years for great earthquakes in the

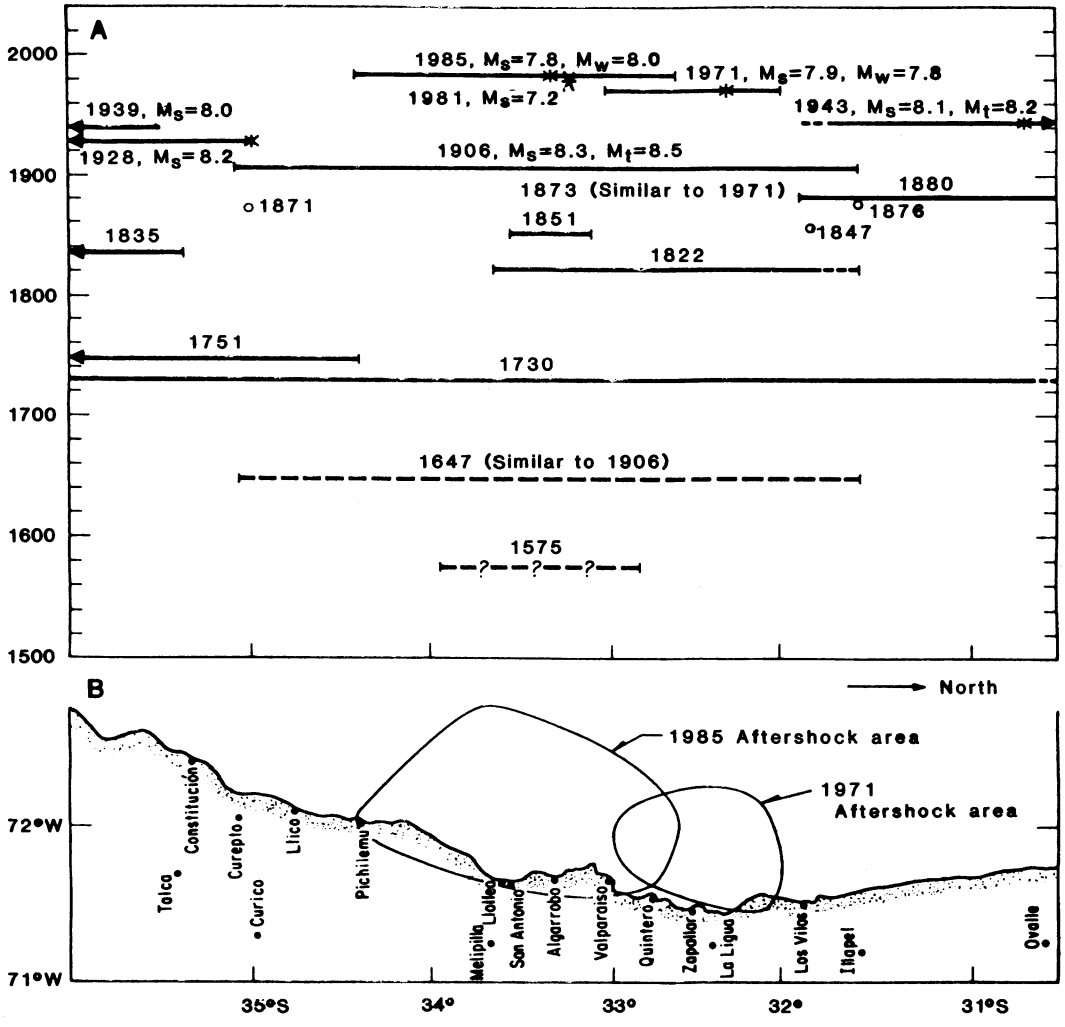


Fig. 3. (A) Space-time diagram of central Chile earthquakes. Solid horizontal lines represent estimated rupture lengths. The arrows indicate that the rupture lengths extended farther in that direction. Dashed lines show uncertain rupture lengths. Dashed line with question marks for the 1575 earthquake reflects inadequate reports, which make the estimated rupture length very uncertain. Earthquakes of past centuries that were large but not great (7.5 > magnitude > 7) and whose rupture lengths could not be estimated are shown by (○). Locations of this century's main shocks are shown by stars. $M_s$, $M_w$, and $M_t$ are surface-wave, moment, and tsunami magnitudes (*16, 25*), respectively. (B) Central Chile region and aftershock areas of the 3 March 1985 and 9 July 1971 earthquakes. International Seismological Center locations were used to define the 1971 aftershock area.

region. Thus, the next great earthquake after the 1906 shock would have been expected in 1989. The earthquake of 1985 fits well with this expectation if we ignore the 1971 earthquake ($M_s$ = 7.9), which had a seismic moment of $0.56 \times 10^{28}$ dyne-cm (*34*) and broke about 110 km of the plate interface (Fig. 3). The aftershock areas of the 1971 and 1985 earthquakes overlap only slightly (Fig. 3), suggesting that different segments of the plate interface were involved in the two ruptures. The sum of the seismic moments of these two earthquakes is about one-fourth that of the 1906 shock.

Our rupture estimates for the 1647, 1730, 1822, 1906, 1971, and 1985 earthquakes are 365, 550, 220 to 250, 365, 110, and 170 km, respectively. We can ignore the 1971 earthquake since past earthquakes of similar size (Fig. 3) were excluded from the recurrence calculation. In other words, we are considering only events with seismic moment $\geq 1 \times 10^{28}$ dyne-cm (rupture length >150 km). We are confident that the record of such earthquakes in the region since the 17th century is complete. When we exclude the 1971 earthquake data, the smallest rupture length is associated with the most recent, better studied 1985 earthquake. Therefore, one might wonder if the rupture lengths of previous earthquakes are not consistently overestimated. On the basis of the extent of damages, the documented coastal uplifts (1822 and 1906 earthquakes), and the tsunami reports (1730 earthquake), this possibility can be definitely ruled out. Thus, we conclude that the rupture lengths of the larger earthquakes offshore central Chile vary by a factor of about 3 and that the 1985 earthquake was the smaller of the sequence. The average displacement on a fault is a linear function of the rupture length (*6*, *35*). Consequently, the average slips associated with the 1647, 1730, 1822, 1906, and 1985 earthquakes are also expected to vary by a factor of 3. The varying rupture lengths and the approximately constant repeat times of these earthquakes cannot be reconciled with the time- or slip-predictable models of earthquake recurrence (*5*, *6*). These models predict constant repeat times for constant slips and variable repeat times for variable slips.

Although the nearly constant repeat time of great earthquakes in the central Chilean region is unique in seismology (*36*) and the 1985 shock may strengthen our confidence in earthquake forecasting, we are unable to explain the observed periodicity in terms of simple physical models. Even without a clear understanding of the physical processes involved, the concepts of seismic gaps and average repeat times (*1*, *2*) remain useful tools in forecasting sites of future earthquakes. The space-time plot in Fig. 3 suggests that the segment south of the 1985 rupture zone is a gap of high seismic potential that may rupture in a great earthquake in the next few tens of years. This observation is supported by the apparent southern migration of rupture areas of great earthquakes over a period of time in central Chile.

## REFERENCES AND NOTES


1. J. A. Kelleher, *J. Geophys. Res.* 77, 2087 (1972).
2. W. R. McCann, S. P. Nishenko, L. R. Sykes, J. Krause, *Pure Appl. Geophys.* 117, 1082 (1979).
3. S. P. Nishenko, *J. Geophys. Res.* 99, 3589 (1985).
4. The earthquake caused 177 deaths and 2575 injuries. It destroyed 70,000 houses and damaged an additional 140,000 dwellings, leaving 950,000 persons homeless. Estimated property damage was about $1.8 billion.
5. K. Shimazaki and T. Nakata, *Geophys. Res. Lett.* 7, 279 (1980).
6. L. R. Sykes and R. C. Quittmeyer, *Am. Geophys. Union Monogr. Earthquake Prediction* (Washington, DC, 1981), pp. 217–247.
7. Alarmed by the intense seismic activity that began on 21 February, a relative of one of us (L.P.) called Mexico City from Valparaíso. Suspecting a possible large earthquake in the region, Mexican seismologists, in collaboration with Chilean colleagues, sought for funds to enable them to travel to Chile with portable field seismographs. The funds did not become available, however, until after the main shock. The first Mexican seismologist arrived in Chile on 5 March with five seismographs. The next day two more seismologists from Mexico arrived with three additional seismographs and two accelerographs.
8. We computed the magnitude of foreshocks and aftershocks from coda duration at PEL (Fig. 1) by using the scale for California, which was developed by W. H. K. Lee, R. E. Bennett, and K. Meager [*U.S. Geol. Surv. Open-File Rep. 28* (1972)]. This scale, although not calibrated for central Chile, provides relative sizes of the events.
9. One of us (R.S.) was in the town of Quintay near the coast of San Antonio (Fig. 1) on 2 March when the water level of the wells serving Quintay decreased by about 2.5 m with respect to the average level expected for that time of year. This change occurred suddenly and had not been observed before by Quintay residents.
10. The National Earthquake Information Service (NEIS) of the U.S. Geological Survey reports a foreshock of $m_b$ 5.2 about 10 seconds before and 7 km northwest of the main shock. The location of the main shock in our data corresponds to the foreshock location reported by NEIS. Since the seismograms from the central Chile network became saturated, it was not possible to locate individual subevents of the main shock.
11. For hypocentral locations of all events, a flat-layer model appropriate for the coastal region [P. Acevedo and M. Pardo, *Rep. Depto. Geología y Geofísica* (Universidad de Chile, Santiago, 1985)] was used. Because of the change in the crustal structure inland, the readings from the permanent stations required corrections. These corrections were found by generating the travel-time curve for a dipping-layer model. In this model the Moho dips 8° inland, a reasonable approximation that fits the poorly known crustal structure given by Acevedo and Pardo. Station corrections were determined for a set of probable hypocenters, and an average station correction found for each station was used in locating aftershocks, main shock, and foreshocks.
12. The focal mechanism of the main shock was provided by G. Ekström (personal communication).
13. The earthquake triggered 36 accelerographs in central Chile, 8 of which were located along the coast. Of these, 26 are operated by the Departamento de Ingeniería Civil and 10 by the Departamento de Geología y Geofísica, both of the Universidad de Chile, Santiago. The coastal accelerograms show higher peak accelerations to the south than to the north (Fig. 1). The maximum peak horizontal (0.67*g*) and vertical accelerations (0.86*g*) were recorded at Llolleo ["Informe Preliminar de los resultados de la red nacional de acelerógrafos para el terremoto del 3 de marzo de 1985," *Reporte del Depto. de Ingeniería Civil* (Universidad de Chile, Santiago, 1985)].
14. G. Plafker (personal communication) conducted a geological reconnaissance of the earthquake and reported a tsunami of 1.2 to 1.8 m between Valparaíso and Cartagena and perhaps one as high as 3 m in Matanza (Fig. 1) within 10 minutes of the main shock and, in some localities, immediately after the earthquake. He also reports a coastal uplift of about 20 cm (near Algarrobo) for 3 to 5 days, which later returned to normal. Plafker, however, found no permanent vertical displacement of the shoreline.
15. The rupture plane of the main shock dips 25° (Fig. 1) toward the continent. Projecting the aftershock locations in Fig. 1 to a 25° dipping plane results in an aftershock area of about 170 by 110 km$^2$, which we also take as the rupture area.
16. Seismic moment of the 1985 earthquake was obtained from G. Ekström, personal communication. $M_0$ is related to moment-magnitude, $M_w$, by log $M_0$ = 1.5 $M_w$ + 16.1 [H. Kanamori, *J. Geophys. Res.* 82, 2981 (1977)].
17. Mercalli intensities differ from modified Mercalli intensities [C. F. Richter, *Elementary Seismology* (Freeman, San Francisco, 1958), p. 136].
18. H. Steffen, *Contribuciones para un Estudio Científico del Terremoto del 16 de Agosto de 1906*, Anales de la Universidad (Imprenta Cervantes, Santiago de Chile, 1907).
19. F. de Montessus de Ballore, *Historia Sísmica de los Andes Meridionales* (Barcelona, Santiago de Chile, 1911–1916). Volume 5 discusses the 16 August 1906 earthquake.
20. C. Lomnitz, *Geol. Rundsch.* 59, 938 (1970).
21. L. Zegers, *El Terremoto del 16 de Agosto*, Anales de la Universidad, Memorias Científicas i Literarias, vol. 119 (Imprenta Cervantes, Santiago de Chile, 1906).
22. F. Montessus de Ballore (*19*) discredited observations of uplift.
23. K. Abe and S. Noguchi, *Phys. Earth Planet. Interiors* 33, 1 (1983). Surface-wave magnitude reported for the 1906 earthquake is 8.1. In this report we based $M_s$ on the current definition used by NEIS, which is 0.18 unit higher than the value one would obtain from the definition used by Abe and Noguchi.
24. Photos of worldwide seismograms are available in E. Rodolph and E. Tams [*Seismogramme des nordpazifischen und Sudamerikanischen Erdbebens am 16 August 1906, Begleitworte und Erlauterungen* (Strassburg, 1907)]. Because an earthquake occurred about 30 minutes earlier in the Aleutians, the seismograms of the 1906 Valparaíso earthquake are contaminated. Nevertheless, surface waves of about a 20-second period for the two earthquakes can be isolated. In determining $M_s$ for the 1906 earthquake, we have used only records from damped seismographs with well-known characteristics.
25. K. Abe, *J. Geophys. Res.* 84, 72 (1981). Tsunami magnitude, $M_t$, and seismic moment, $M_0$, are related by log $M_0$ = 1.5 $M_t$ + 16.1.
26. Tsunami data for the 1985 earthquake are given by G. Burton and W. Person in *Eos* 66, 437 (1985). The values, listed as peak-to-trough amplitudes, are actually maximum amplitudes with respect to the mean sea level, that is, zero to maximum (G. Pararas-Carayannis, personal communication).
27. H. Kanamori and J. J. Cipar, *Phys. Earth Planet. Interiors* 9, 128 (1974).
28. The calibration with respect to the 1985 and 1960 earthquakes gives $M_t$ values for the 1906 earthquake of 8.55 (Hilo), 8.39 (Honolulu), and 8.50 (Japan). The average $M_t$ is 8.48 with the corresponding $M_0$ of $6.6 \times 10^{28}$ dyne-cm.
29. A. Perrey, *Documents relatifs aux tremblements de terre au Chili*, Ann. Soc. Imper. d'Agric. (Barret, Lyon, 1854).
30. F. Greve, *Descripción de los principales efectos producidos por los sismos destructores en Chile y ubicación de sus epicentros* (Instituto Sismológico, Universidad de Chile, Santiago, 1953).
31. Nishenko (*3*) gives a rupture length of 350 to 450 km for the 1730 earthquake. We believe our estimate of 550 km is more realistic in view of the damage and tsunami reports.
32. C. Darwin [*Geological Observations on Coral Reefs, Volcanic Islands and on South America: Being the Geology of the Voyage of the Beagle Under the Command of Captain FitzRoy, R.N., During the Years 1832 to 1836*] in 1835 reported an uplift of 0.9 to 1.2 m at the mouth of the Rapel River (33.9°S). C. Davison [*Great Earthquakes* (Murby, London, 1936)] associates this uplift with the 1822 earthquake. We believe this association is doubtful.

33. M. Graham, *Trans. Geol. Soc. London* (Ser. 2) **1**, 413 (1824).
34. M. Malgrange, A. Deschamps, R. Madariaga, *Geophys. J. R. Astron. Soc.* **66**, 313 (1981).
35. C. Scholz, *Bull. Seismol. Soc. Am.* **72**, 1 (1982).
36. A remarkable periodic main shock sequence has been reported for Parkfield, California, by W. H. Bakun and T. V. McEvilly [*J. Geophys. Res.* **89**, 3051 (1984)]. The ruptures involved in Parkfield main shocks, however, are only 20 to 30 km in length.
37. We thank A. Giesecke for obtaining Unesco support; H. Fuenzalida for encouragement and field support; I. Herrera and L. Esteva for facilitating the trip to Chile of Mexican seismologists and for financial support; J. Campos, C. Droguett, S. Droguett, A. Fuenzalida, A. Giavelli, and many others for help in fieldwork; F. Espinoza for tide data; and M. Ulloa and D. Haro for technical assistance. Field support from government authorities in Chile is gratefully acknowledged. We thank C. Lomnitz and H. Kanamori for comments and revision of the manuscript.

26 August 1985; accepted 21 March 1986

# High Potassium Conductance in Astrocyte Endfeet

ERIC A. NEWMAN

**The distribution of potassium conductance over the surface of freshly dissociated salamander astrocytes was determined by monitoring cell depolarizations evoked by focal increases in the extracellular potassium concentration. The specific potassium conductance of the endfoot processes of these cells was approximately tenfold higher than the conductance of other cell regions. This dramatically nonuniform conductance distribution may play an important role in the regulation of extracellular potassium levels by glia in the brain.**

ALTHOUGH ASTROCYTES OUTNUMBER all other types of glial cells and neurons in the vertebrate brain, their membrane properties and functions are not well understood (*1, 2*). Müller cells, the principal glial cells of the retina, resemble astrocytes in many respects. In Müller cells, 95 percent of the total cell membrane conductance is localized to the cell's endfoot process (*3, 4*). It is not known whether this striking membrane specialization occurs only in these specialized retinal cells or whether membrane conductance is also distributed nonuniformly across the surface of all astrocytes throughout the brain. I have addressed this issue by determining the distribution of potassium conductance over the surface of freshly dissociated astrocytes.

Astrocytes were isolated from the optic nerve of the salamander *Ambystoma tigrinum*. Optic nerves were excised with the meninges intact and partially teased apart before incubation in papain [0.6 mg/ml in Hepes-buffered Ringer solution; see (*4*) for composition of Ringer solutions] for 30 minutes at 28°C. They were then washed several times in Hepes-Ringer and maintained at 0°C for 3 to 4 hours before the cells were dissociated by gentle trituration. Isolated cells were placed in a recording chamber and perfused with a bicarbonate-buffered Ringer solution (containing 2.5 m*M* $K^+$) maintained at 15°C. Experiments were performed on cells within 2 hours of dissociation.

The cells isolated with this dissociation procedure all had a similar appearance. They had several stout, branching processes radiating from a prominent soma. These cells were provisionally identified as astrocytes on the basis of their appearance and because astrocytes are the principal cell type found in the salamander optic nerve. [Amphibian optic nerves contain no intrinsic neurons and few myelinated fibers or oligodendrocytes (*5, 6*).] The radial processes of these cells terminated in bulbous enlargements. These were the endfeet, which lie at the ends of astrocyte processes in the intact brain and optic nerve. Cells had from 3 to 17 endfeet each, although the exact number was sometimes difficult to determine (mean = 8.7; $n = 30$). Some radial processes lacked endfeet, probably because they were broken off during dissociation.

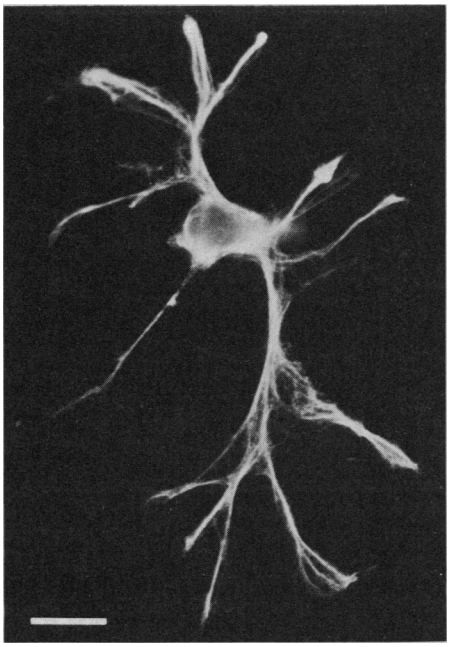

Fig. 1. GFAP immunoreactivity of a freshly dissociated cell from the optic nerve of the salamander (*19*). This fluorescence micrograph shows that the cell was heavily labeled with antibodies to GFAP, identifying it unequivocally as an astrocyte. Scale bar, 20 μm.

Dissociated cells were characterized by immunofluorescent labeling of glial fibrillary acidic protein (GFAP), a characteristic cytoplasmic marker of astrocytes (*7*). All dissociated cells were labeled heavily with monoclonal antibodies to GFAP (Fig. 1), identifying them conclusively as astrocytes. Control cells, in which saline was substituted for the primary GFAP antibody, remained unlabeled. In a second series of controls, dissociated cells from the salamander retina were tested for GFAP immunoreactivity. Retinal neurons and photoreceptors showed no signs of labeling, while Müller cells [which contain GFAP (*8*)] were heavily labeled.

Whole cell intracellular recordings were made from the somata of freshly dissociated astrocytes with patch clamp microelectrodes filled with 125 m*M* KCl (*4*). For cells in which the membrane potential had stabilized, the cell resting potential was $-87.3 \pm 1.9$ mV (mean ± SD; $n = 12$). The cell input conductance, measured by injecting 50 to 100 pA depolarizing current pulses through the recording microelectrode, averaged 25.1 ± 18.3 nS and ranged from 6.0 to 55.6 nS (71 ± 49 Mohms; $n = 12$).

Astrocytes are known to be almost exclusively permeable to $K^+$ at or near their resting potential (*5, 9*). It is not known, however, whether this $K^+$ conductance is distributed uniformly over the cell surface or whether it is localized to particular regions (*4*). Regional differences in membrane $K^+$ conductance were measured by monitoring the cell membrane potential as the extracellular $K^+$ concentration ($[K^+]_o$) was raised over localized regions of the cell surface (*4*). Recordings were made with patch clamp electrodes attached to cell somata. Localized $K^+$ increases were generated by pressure ejection of a 125 m*M* KCl solution from a second, extracellular micropipette positioned against the cell surface.

When $K^+$ was ejected onto the endfeet of the cell (Fig. 2, traces a, b, g, and h) large depolarizations were recorded. In contrast, much smaller depolarizations were evoked when $K^+$ was ejected onto the radial processes of the cell (Fig. 2, traces c, d, and f) or onto the soma (Fig. 2, trace e). The ejected

Eye Research Institute of Retina Foundation, 20 Staniford Street, Boston, MA 02114.